PD-1–Dependent Modulation of Sensory Neurons by a *Staphylococcus epidermidis* Lipoteichoic Acid Drives Analgesia

*Zhiqiang Liu[1], Yen-Hsin Cheng[2], Catherine V. Osborn[1], Marco Martina[2], Anthony J. Schaeffer[1], and Praveen Thumbikat[1]**

[1]Department of Urology, [2]Department of Neuroscience, Northwestern University Feinberg School of Medicine, Chicago, IL

* Corresponding Author: Praveen Thumbikat, D.V.M, Ph.D., Professor, Department of Urology, Feinberg School of Medicine, Searle 12-562, 320 E. Superior St., Chicago, IL 60611. Phone: (312) 503-1050; e-mail: thumbikat@northwestern.edu; https://orcid.org/0000-0002-5454-4172

Running Head: SELTA Analgesia via Neuronal PD-1

Keywords: PD-1, sensory neurons, analgesia, *Staphylococcus epidermidis*, lipoteichoic acid, SELTA, neuroimmune modulation, chronic pain

AUTHOR CONTRIBUTIONS: Zhiqiang Liu – performed experiments and data acquisition, data analysis and manuscript writing, Yen-Hsin Cheng – assisted with neuronal experiments and analyses. Catherine V. Osborn – assisted with experimental work and data processing. Marco Martina – contributed to data interpretation and neuronal physiology insights. Anthony Schaeffer – contributed to study design and interpretation. Praveen Thumbikat – directed the study, supervised all aspects, analyzed data, and wrote the manuscript.

DATA AVAILABILITY: All data generated in this study are available from the corresponding author upon request.

ACKNOWLEDGMENTS: Funding sources supporting this work included NIH/NIDDK grants R01DK108127, along with Northwestern University core resources.

Conflicts of interest: Dr. Praveen Thumbikat and Dr. Anthony J. Schaeffer are inventors on a Northwestern University–owned patent related to the SELTA molecule described in this manuscript. Both authors are co-founders of Equilibrio Biosciences Inc., a startup company interested in SELTA-based therapeutic development. These interests did not influence the design, conduct, or interpretation of the study. All other authors declare no competing interests.

Abstract

The immune checkpoint receptor PD-1, traditionally known for suppressing T-cell activation, is also expressed in peripheral sensory neurons where it limits excitability, but the physiological contexts in which neuronal PD-1 is engaged remain poorly defined. We previously identified a purified *Staphylococcus epidermidis* lipoteichoic acid analog (SELTA) that rapidly alleviates pelvic pain in mice. Here, we investigated whether SELTA functions as an exogenous activator of neuronal PD-1 and whether PD-1 is required for its analgesic effects. SELTA increased *Pdcd1* transcripts and PD-1 protein in dorsal root ganglion (DRG) neurons and prostate-innervating sensory fibers, and colocalized with TLR2 at neuronal membranes where it enhanced PD-1 Y248 phosphorylation. In primary DRG cultures, SELTA suppressed ATP-evoked Ca^{2+} responses, indicating reduced neuronal excitability. This effect was abolished by PD-1 neutralization but restored when neutralization was blocked by a PD-1 control peptide, demonstrating both PD-1 dependence and specificity. In male mice with chronic pelvic allodynia induced by experimental autoimmune prostatitis, intraurethral SELTA produced robust, concentration-dependent, and repeatable reductions in tactile hypersensitivity. Sensory neuron–specific PD-1 conditional knockout mice showed normal baseline behavior but failed to respond to SELTA, confirming that PD-1 expression in nociceptors is essential for SELTA-mediated analgesia. These findings identify SELTA as a commensal-derived activator of neuronal PD-1 signaling. Through TLR2 engagement, PD-1 phosphorylation, and suppression of excitatory calcium signaling, SELTA attenuates nociceptor activation and reduces pelvic pain. This mechanism highlights neuronal PD-1 as a modifiable checkpoint pathway and a promising non-opioid target for chronic pain therapy.

Introduction

Chronic pelvic pain syndromes, including chronic prostatitis/chronic pelvic pain syndrome (CP/CPPS), remain difficult to treat and are marked by persistent nociceptive sensitization [4; 5; 29; 33]. Although pro-inflammatory pathways contributing to pelvic pain have been studied [19], the endogenous inhibitory mechanisms that actively restrain nociceptor activity are less well understood. Identifying such pathways is critical for developing non-opioid strategies for chronic pelvic pain.

Recent work has revealed that the immune checkpoint receptor programmed cell death-1 (PD-1), classically known for regulating T-cell activation, is also expressed in sensory neurons where it suppresses neuronal excitability [3; 10; 36]. Endogenous PD-1 ligands such as PD-L1 reduce nociceptor firing, while PD-1 blockade increases pain sensitivity in both animal models and patients receiving immune checkpoint inhibitors [7; 13]. Despite this, the physiological contexts in which neuronal PD-1 is engaged, and whether exogenous ligands can activate this pathway, remain largely unknown.

Our laboratory previously reported that a lipoteichoic acid (LTA) molecule purified from a commensal *Staphylococcus epidermidis* strain produces rapid and robust analgesia in murine models of pelvic pain [16-18]. This molecule, termed SELTA, is structurally distinct from LTAs of pathogenic *S. aureus*, is immunomodulatory, and acts with a kinetics suggesting direct neuronal modulation. These findings align with broader evidence that *S. epidermidis*-derived molecules can shape host epithelial and immune signaling [11; 20], raising the possibility that commensal factors may also influence neuroimmune interactions.

Given the known inhibitory role of PD-1 in sensory neurons, we hypothesized that SELTA may function as an exogenous activator of neuronal PD-1, distinct from canonical endogenous ligands. In this study, we examined whether SELTA regulates PD-1 expression and phosphorylation in dorsal root ganglion (DRG) neurons and tested whether sensory-neuron-specific deletion of PD-1 abolishes SELTA-mediated analgesia. Our findings demonstrate that SELTA engages a TLR2–PD-1 signaling axis, activates PD-1 through Y248 phosphorylation, and requires neuronal PD-1 to reduce pain, identifying a commensal-derived activator of a neuronal immune checkpoint pathway.

Materials and Methods

Ethics statement: All animal procedures were approved by the Institutional Animal Care and Use Committee (IACUC) at Northwestern University (protocols IS00021559 and IS00003610). The IACUC at Northwestern is AAALAC accredited, and Northwestern University has an Animal Welfare Assurance on file with the Office of Laboratory Animal Welfare (A3283-01). All studies were conducted in accordance with United States Public Health Service regulations, the Animal Welfare Act, and applicable federal and local laws.

Animals: All procedures were approved and monitored by the Northwestern University IACUC. Pain-related experiments were conducted in accordance with the IASP Guidelines for the Use of Animals in Research (January 2014). Male C57BL/6 (B6) mice (6–8 weeks old; Jackson Laboratory, Bar Harbor, ME) were housed with ad libitum access to sterilized food and water. Unless otherwise indicated, 4–5 mice were used per group, and experiments were performed in duplicate or triplicate (N = 2–3) with no exclusion of animals.

Induction of experimental autoimmune prostatitis (EAP)

EAP was induced in C57BL/6 mice by subcutaneous injection behind the shoulder of a 1:1 emulsion of rat prostate homogenate and TiterMax® adjuvant, as described previously [23]. Pelvic tactile allodynia was assessed using von Frey filament testing (section 2.5). Unless otherwise specified, testing was performed at baseline (prior to EAP induction) and at 7-day intervals thereafter. Experimental endpoints were at day 28 or day 120 post-EAP induction. Results were expressed as percentage change relative to baseline, and for each von Frey filament, responses were averaged within each group. Behavioral testing was performed by an experimenter blinded to treatment allocation. At designated endpoints, mice were euthanized and the prostate, lumbar and sacral DRG, and corresponding spinal cord segments were harvested for analysis.

Generation of sensory neuron–specific Pdcd1 conditional knockout mice: Sensory neuron–specific Pdcd1 conditional knockout mice were generated using a Cre–loxP strategy. Pdcd1^flox/flox^ mice harboring loxP sites flanking critical exons of the Pdcd1 gene (gift of Dr. Vassiliki A. Boussiotis) [1] were crossed with Advillin-Cre transgenic mice (Jackson Laboratory, stock #032536), which express Cre recombinase under the sensory neuron–specific Advillin promoter. Offspring were genotyped to identify mice homozygous for the floxed Pdcd1 allele and heterozygous for Cre (Pdcd1^f/f^;Advillin-Cre^+/-^). Genomic DNA was extracted from tail biopsies. PCR was performed using the following primers:

- Pdcd1 floxed allele:
    - Forward: 5′-TATCCCTGTATTGCTGCTGCTG-3′

- Reverse:5′-AATGAATTGAGGAGTAGGGCCTG-3′

  (387 bp wild-type; 490 bp floxed)

- Cre transgene:
  - Forward: 5′-AATGGCTCCCTGTTC ACTGT-3′
  - Reverse WT: 5′-TGACTAGGTAGAGGTGCAAATGTC-3′ (530 bp wild type)
  - Reverse Cre: 5′-AGGCAAATTTTGGTGTACGG-3′ (150 bp transgene)

PCR products were resolved on 1.5% agarose gels. For validation, DRG sensory neurons from Pdcd1^f/f^;Advillin-Cre^+/-^ and Pdcd1^f/f^ littermates were analyzed for PD-1 expression by qPCR and immunohistochemistry to confirm loss of PD-1 in neurons and preservation in non-neuronal cells.

Mechanical allodynia: Mechanical hypersensitivity was assessed as described previously [24]. Mice were tested prior to prostate antigen (PAg) injection (baseline) and after development of EAP. Referred tactile allodynia was evaluated using von Frey filaments applied to the lower abdomen [12]. Mice were placed individually in Plexiglas chambers (6 × 10 × 12 cm) on a stainless-steel wire grid floor and allowed to acclimate for 20 min. Testing was performed under standardized conditions (fixed time of day, single experimenter, blinded to group). Five filaments (0.04, 0.16, 0.4, 1.0, and 4.0 g; Stoelting, USA) were applied in ascending order of force. Each filament was applied for 1–2 s with 5 s inter-stimulus intervals, for a total of 10 applications per filament. Stimulation was confined to the lower abdomen overlying the prostate. A positive response was defined as one of the following: (1) sharp retraction of the abdomen, (2) immediate licking or scratching at the stimulus site, or (3) jumping. Response frequency was calculated as the

percentage of positive responses out of 10 stimulations (e.g., 5/10 = 50%). Data are presented as mean percentage response frequency ± SEM. Percentage change from baseline was calculated for each time point and filament.

Additional Behavioral tests: The animals were acclimated to the testing room environment for at least 2 days prior to the first test. The tests were performed during the light cycle. Animals had free access to food and water. Each test was video recorded by a digital camera connected to ANY-maze software (Stoelting Co, IL, USA). The data were analyzed using ANY-maze software. GraphPad Prism software (GraphPad Software, MA, USA) was used for statistical analysis. The tests were performed in this order: Dark and Light Box, Y maze, Novel Object Recognition and Open Field.

Dark and Light Box test: The animals are tested in a 40 x 40 cm box made of black plexiglass. This box is divided into 2 equal-sized chambers which are connected by a small opening, so the studied mouse can freely move between the 2 chambers. One of the chambers is covered (and dark) while the other is exposed to the light. The covered chamber is normally preferred by mice. A mouse is placed into the open side and the test lasts 5 minutes. We measured how much time the mouse spends in each chamber and the distance travelled in the light side. The preference for the light side is expressed as percentage: (time spent in light chamber/total testing time) x 100.

Y-maze spontaneous alteration test: Testing was done in a Y-shaped maze with three - high-walled (10 cm tall) arms at a 120° angle from each other. After being placed in the center of the maze, the mouse was allowed to freely explore the three arms for 5 minutes. Over the course of multiple arm entries, mice show a tendency to enter a less recently visited arm [14]. An entry is defined when all four limbs are within the arm. The sequence

of arm entries is recorded, and the number of spontaneous alterations is calculated. A spontaneous alteration occurs when the mouse enters different arms in 3 consecutive entries. results are presented as percentage of correct spontaneous alterations: (number of the spontaneous alterations/the total number of entries – 2) × 100.

Novel object recognition test (NOR): NOR is a classic test of episodic memory [8]. Mice are habituated to an empty boxed arena (50 x 50 cm) for 1 hr. On the next day, during the acquisition trial, mice are allowed to explore two identical objects for 10 min and are then returned to the home cage. On the next day, for the NOR retention trial, mice are exposed to one familiar object and one novel object. We quantified the fraction of time spent exploring each object in each trial, and the distance traveled. The Discrimination index is expressed as: (time spent exploring the novel object – time spent exploring the familiar object)/total exploration time.

Open Field test: This test is widely used to assess exploratory behavior and general activity in rodents. We placed the mouse under study in a square boxed arena (40 x 40 cm) for 5 minutes. We quantified total distance travelled, and the time spent in the arena center vs. wall-hugging (thigmotaxis), which is a commonly used index of anxiety [26]. The ANY-maze software dissects the total space into 9 equal-sized squares, which therefore identifies the center square. The preference for the central area is expressed as a percentage: (time spent in middle/total test time) x 100

Ex vivo DRG culture: Ex vivo DRG cultures were prepared with minor modifications of published protocols [15; 25; 27; 28]. Briefly, 5–7-week-old C57BL/6 mice were euthanized with a lethal dose of isoflurane. Under aseptic conditions, the vertebral column from sacral to lumbar levels was exposed, and the spinal canal was opened along the midline. DRG

(L2–S1) were dissected using #7 forceps, rinsed twice in sterile HBSS, and transferred to 96-well plates containing 200 µl DMEM supplemented with 10% FBS, 2% B27, and 10 ng/ml NGF. DRG were cultured at 37°C, 5% CO_2 for 24 h with or without 100 ng/ml SELTA.

Primary DRG sensory neuron culture and *in vitro* inflammatory stimulation: DRG were dissected from C57BL/6 mice into cold HBSS and minced into ~0.2-mm fragments. After centrifugation at 100 g for 1 min, tissue was digested with papain (20 min, 37°C) followed by collagenase/dispase (20 min, 37°C). Cells were centrifuged at 400 g for 4 min and resuspended in L-15 medium containing 5% FCS, penicillin/streptomycin, and HEPES. Neurons were enriched using a Percoll gradient (1300 g, 10 min), then resuspended in F12/DMEM containing 10% FCS, 10 ng/ml 2.5S NGF, penicillin/streptomycin, and HEPES. Cells were plated at 5×10^3 neurons per well in 4-chamber glass-bottom dishes (D35C4-20-0-N; Cellvis) for subsequent experiments.

For in vitro inflammatory stimulation, neurons were treated with recombinant TNF-α (10 ng/ml) for 12-18 hours prior to experimental assays. This exposure paradigm was selected based on prior studies demonstrating a significant role for TNF-α signaling in dorsal root ganglion neurons following peripheral nerve injury [6; 9; 31] and the use of prolonged TNF-α treatment to model neuropathic and inflammatory pain–associated neuronal states in vitro [30; 32]. Chronic TNF-α exposure has been shown to induce transcriptional and protein-level changes in sensory neurons, including increased expression of the voltage-gated sodium channel NaV1.7, which is upregulated in models of nerve injury–associated pain [30].

Calcium imaging: Calcium imaging was performed as described previously [22]. DRG neuron cultures exposed to inflammatory stimulation were loaded with 1 µM Fura-2 AM

and 1 μM Pluronic F-127 (Life Technologies) in HBSS (pH 7.4; 137 mM NaCl, 5.4 mM KCl, 1.3 mM $CaCl_2$, 0.5 mM $MgCl_2$, 0.4 mM $MgSO_4$, 4.2 mM $NaHCO_3$, 0.44 mM KH_2PO_4, 0.34 mM Na_2HPO_4, 5.5 mM glucose, 25 mM HEPES, 1 mg/ml BSA) at 37°C for 30 min, then washed in HBSS . For SELTA experiments, neurons were incubated with SELTA alone, SELTA plus rat anti-PD-1 neutralizing antibody, or SELTA plus PD-1 control peptide and anti-PD-1 antibody and returned to the incubator for ≥10 min before recording. Cells were transferred to the imaging setup and equilibrated to room temperature. Baseline intracellular Ca^{2+} levels were recorded for at least 60 s using ratiometric imaging at 340/380-nm excitation, followed by ATP stimulation. Signals were recorded for up to 600 s. At the end of each experiment, 2 μM ionomycin was applied to elicit a maximal Ca^{2+} response and confirm cell viability. For each chamber, ~10–80 cells were imaged using a Leica DMI6000B microscope with a 40× oil-immersion objective and experiments were repeated three times with independent cultures. Images were captured with a Hamamatsu CCD camera and analyzed using MetaFluor (Molecular Devices). F340/F380 ratios were used to quantify Ca^{2+} responses.

RT-PCR and qPCR: RNA was isolated from iliac lymph nodes, splenocytes, and cultured sensory neurons as described [18]. RNA concentration was measured using a Spark microplate reader (Tecan). cDNA was synthesized with SuperScript® III First-Strand Synthesis System (Invitrogen) according to the manufacturer's protocol. qRT-PCR was performed using SsoAdvanced™ Universal SYBR® Green Supermix (Bio-Rad) with 50 ng cDNA per 25-μl reaction on a CFX Connect™ Real-Time PCR Detection System (Bio-Rad). Primers were designed using the IDT PrimerQuest™ Tool. Relative expression was calculated using the ΔΔCt method with appropriate internal controls. Samples were run

in biological triplicate (3–4 mice per group) with technical replicates. Primer sequences for full-length Pdcd1 and splice variants are listed in Tables 1 and 2.

Immunohistochemistry and immunofluorescence: Mice were anesthetized with 2.5% isoflurane (Isothesia; Butler) and transcardially perfused with cold PBS followed by 4% paraformaldehyde (PFA). DRG and prostates were removed and post-fixed in 4% PFA (DRG, 1 h; prostate, 24 h), then cryoprotected in 30% sucrose overnight. Tissues were embedded in OCT (Tissue-Tek), frozen in dry ice–chilled isopentane, and stored at −80°C. L2–S1 DRG and prostate were sectioned at 10 µm on a cryostat (Leica), mounted on Superfrost Plus slides, and stored at −80°C. Sections were fixed in 4% PFA for 10 min, subjected to antigen retrieval in 10 mM sodium citrate buffer (pH 9.0) for 10 min at 80°C, and blocked in 0.3% Triton X-100/5% donkey serum in PBS for 30 min. Primary antibodies were applied overnight at 4°C in blocking buffer, followed by three 10-min PBS washes and 2-h incubation with Alexa Fluor 405-, 488-, 555-, or 647-conjugated secondary antibodies. Nuclear counterstaining was performed with Hoechst 33342 or DAPI, and sections were mounted in ProLong Diamond Antifade (Invitrogen). Primary antibodies included rabbit anti-PD-1 (1:1000, Sigma-Aldrich PRS4065), rabbit anti-phospho-PD-1 (1:500, Abcam), mouse anti-CGRP (1:1000, Abcam), rabbit anti-CGRP (1:500, Cell Signaling ab81887), goat anti-IBA1 (1:1000, Novus), guinea pig anti-NeuN (1:2000, Synaptic Systems), chicken anti-βIII-tubulin (1:500, Novus), goat anti-TLR2 (1:500, Santa Cruz), and mouse anti-lipoteichoic acid (1:50, Thermo Fisher). SELTA used for experiments (100 ng/ml) was extracted from a unique strain of *S. epidermidis* isolated from the prostate of a healthy human volunteer at Northwestern University [18] and purified at the Complex Carbohydrate Research Center (CCRC) at the University of

Georgia. SELTA characterization and purity were confirmed using H-NMR analysis at the CCRC.

Confocal imaging and quantitative immunofluorescence: Images were acquired on a Nikon A1 confocal microscope using Plan Apo 20× (NA 0.75) and 60× oil (NA 1.4) objectives. Comparable regions were imaged across animals, and acquisition parameters were standardized using a predefined template. Noise reduction was performed in ImageJ. Regions of interest (ROIs) were defined by NeuN immunoreactivity to identify neuronal cell bodies. The same ROIs were applied to PD-1 and phospho-PD-1 channels to extract mean fluorescence intensity. For cell size–dependent analyses, DRG neurons were classified as small (<300 μm²), medium (300–500 μm²), or large (>500 μm²).

Mouse Pdcd1 RNA fluorescence in situ hybridization with PD-1 immunostaining: Custom Stellaris® FISH probes were designed against mouse Cd279 (Pdcd1) mRNA (NM_008798) using the Stellaris Probe Designer (Biosearch Technologies). The probe set consisted of 48 TAMRA-labeled oligonucleotides complementary to full-length Cd279 and its variants. Prostate and DRG sections (10 μm) from naïve and EAP-treated mice were thawed, fixed in 3.7% formaldehyde in PBS for 10 min, washed twice in PBS, and permeabilized in 70% ethanol for 1 h. Slides were rinsed in Wash Buffer A (Biosearch) and incubated overnight at 37°C with FISH probes and primary antibodies in hybridization buffer. After hybridization, samples were washed in Wash Buffer A, incubated with DAPI and Cy5-conjugated secondary antibodies for 2 h, rinsed in Wash Buffer B (Biosearch), and coverslipped with Vectashield (Vector Laboratories) for imaging.

Statistical analysis: Statistical analyses were performed using GraphPad Prism™ and Microsoft Excel™. Data are presented as mean ± SD unless otherwise indicated.

Comparisons between two groups used Student's t test. Comparisons involving more than two groups used one-way or two-way ANOVA, as appropriate, followed by Tukey's or Bonferroni's post hoc tests. A p value < 0.05 was considered statistically significant.

Results

SELTA increases neuronal PD-1 expression in sensory ganglia

To define the distribution of PD-1 across tissues relevant to pain signaling, we first assessed *Pdcd1* transcript levels by RT-PCR. Baseline *Pdcd1* expression was detected in immune organs (spleen, lymph nodes) and prostate, as well as throughout the sensory and central nervous system, including dorsal root ganglia (DRG), spinal cord, thalamus, hippocampus, and cortex (Fig. 1A). We next examined whether intraurethral SELTA administration impacted PD-1 expression in sensory neurons. qPCR analysis demonstrated that *Pdcd1* mRNA was significantly increased in lumbosacral DRG following SELTA exposure compared with controls (Fig. 1B).

To determine whether SELTA also modulates PD-1 protein levels, we evaluated PD-1 immunoreactivity in an ex vivo DRG preparation. SELTA treatment (100 ng/mL, 24 h) increased PD-1 signal intensity relative to untreated cultures (Fig. 1C). Stratification by neuronal size showed that SELTA elevated PD-1 across small-, medium-, and large-diameter neurons (Fig. 1D&E). Quantification confirmed a significant increase in overall PD-1 immunoreactivity (Fig. 1F), and normalization to NeuN indicated a more pronounced increase in medium- and large-diameter neurons (Fig. 1G).

To confirm that SELTA-induced PD-1 expression arises directly from sensory neurons rather than from non-neuronal cells that may reside in DRG (e.g., glia or patrolling immune

cells), we examined purified DRG neurons in vitro. In this fully neuronal culture system, SELTA increased *Pdcd1* expression irrespective of the presence of TNFα, indicating that SELTA can directly upregulate PD-1 in sensory neurons independent of inflammatory cytokines (Supplementary Fig. S1B). Because *Pdcd1* encodes multiple splice variants, we further quantified isoform-specific transcription under thapsigargin-induced ER stress. SELTA significantly increased total *Pdcd1* and selectively enhanced the *Pdcd1Δex3* splice variant, whereas other variants remained at or below detection (Supplementary Fig. S1C–D). Together, these findings show that PD-1 is natively expressed in both immune and sensory tissues and that SELTA upregulates neuronal PD-1 expression directly in sensory neurons, affecting both total *Pdcd1* and specific transcript variants.

SELTA binding to TLR2 increases PD-1 phosphorylation in sensory neurons

Because SELTA increased total PD-1 expression in DRG neurons, we next examined whether SELTA directly engages neuronal receptors to activate PD-1–associated signaling. Confocal imaging demonstrated that exogenous SELTA localized to neuronal somata and synapse-like regions where it colocalized with TLR2 and phosphorylated PD-1 (pPD-1) (Fig. 2A).

Using an ex vivo DRG preparation, SELTA treatment (100 ng/mL, 24 h) significantly increased pPD-1 immunoreactivity compared with untreated cultures (Fig. 2B). This effect was observed across neuronal size classes (Fig. 2C) and remained significant after normalization to NeuN (Fig. 2D), indicating that SELTA enhances PD-1 phosphorylation independent of neuronal number. These findings demonstrate that SELTA engages TLR2 on sensory neurons and increases PD-1 phosphorylation, consistent with activation of an early signaling step downstream of receptor engagement.

SELTA attenuates pelvic allodynia in EAP mice with both single and repeated dosing and shows a concentration-dependent effect

Following EAP induction, mice developed progressive pelvic tactile allodynia, with response frequencies increasing through day 21 before reaching a plateau (Fig. 3A–C). Intraurethral SELTA administration at day 21 significantly reduced pelvic allodynia compared with untreated EAP controls, with improvements evident within one week (Fig. 3B). This analgesic effect gradually diminished, and a second SELTA instillation at day 70 again reduced pelvic hypersensitivity (Fig. 3C), demonstrating that SELTA's effect is reproducible with repeated dosing.

To assess concentration dependence, EAP mice received a single intraurethral SELTA dose across a 10,000-fold concentration range. SELTA produced a graded reduction in pelvic hypersensitivity, with higher concentrations producing greater attenuation (Fig. 3D). These findings show that SELTA reduces EAP-induced pelvic allodynia after both single and repeated dosing and that its analgesic activity is concentration dependent.

SELTA increases PD-1 expression in prostate nerve fibers of EAP mice

To evaluate whether SELTA enhances PD-1 expression at peripheral nociceptive targets, we examined the prostate—a tissue extensively innervated and directly affected in EAP. RNA in situ hybridization demonstrated increased *Pdcd1* mRNA in prostates of SELTA-treated EAP mice compared with EAP-only controls (Fig. 4A). Corresponding increases in PD-1 protein were observed in adjacent sections.

Immunofluorescent labeling revealed greater PD-1 colocalization with βIII-tubulin–positive nerve fibers in the stromal compartment of SELTA-treated prostates (Fig. 4B),

with high-magnification images confirming PD-1 enrichment in nerve bundles and terminals near the epithelial border. Blood-derived immune cells with high PD-1 expression were occasionally observed within the lumen. SELTA-treated mice also showed increased PD-1 colocalization with CGRP-positive sensory fibers (Fig. 4C). Together, these findings indicate that SELTA enhances PD-1 expression in both general neuronal and nociceptive sensory fibers innervating the prostate.

Sensory neuron–specific deletion of PD-1 abolishes SELTA-induced analgesia in EAP mice

To determine whether neuronal PD-1 is required for SELTA-mediated analgesia, we generated sensory neuron–specific PD-1 conditional knockout (CKO) mice by crossing *Pdcd1* floxed mice with Advillin-Cre drivers (Fig. 5A). Immunofluorescence confirmed loss of PD-1 in NeuN-positive DRG neurons of PD-1$^{f/f}$;Advillin-Cre mice while preserving PD-1 expression in IBA-1–positive macrophages/glia (Fig. 5B), demonstrating successful and neuron-specific deletion.

Baseline and EAP induced behavioral assessments showed no differences between WT and CKO mice in anxiety-like behavior, locomotor activity, exploratory behavior, or recognition memory (Supplementary Fig. S2; n = 9/group), ensuring that pain measurements would not be confounded by general behavioral deficits.

EAP was induced in both genotypes and allowed to develop for 50 days before intraurethral SELTA administration. In WT mice, SELTA produced rapid and sustained reductions in pelvic tactile allodynia at 1-, 3-, 5-, and 7-days post-treatment (Fig. 6A). In contrast, CKO mice showed no improvement following SELTA instillation (Fig. 6B).

Comparison of treatment effects demonstrated a marked loss of SELTA responsiveness in CKO mice (Fig. 6C). These findings demonstrate that PD-1 expression in sensory neurons is essential for SELTA-induced analgesia in EAP.

SELTA suppresses ATP-evoked calcium signaling in DRG neurons through a PD-1–dependent and PD-1–specific mechanism

To determine whether SELTA functionally modulates sensory neuron activation, we examined ATP-induced intracellular calcium responses in primary DRG neurons. SELTA pretreatment markedly reduced ATP-evoked Ca^{2+} elevations, indicating suppression of neuronal excitability (Fig. 7A). Neutralization of PD-1 with a blocking antibody abolished this effect, restoring ATP-induced Ca^{2+} responses to control levels (Fig. 7B). Pre-incubation of the PD-1 antibody with a PD-1 control peptide prevented effective neutralization and restored SELTA's inhibitory effect on ATP-induced Ca^{2+} signaling (Fig. 7C–D).

These findings demonstrate that SELTA suppresses sensory neuron calcium mobilization in a PD-1–dependent and PD-1–specific manner, identifying neuronal PD-1 signaling as a key functional mediator of SELTA-induced reductions in sensory neuron activation.

Discussion

The present study identifies a neuroimmune mechanism in which SELTA, a lipoteichoic acid analog purified from a commensal *Staphylococcus epidermidis* strain, activates PD-1 signaling in sensory neurons to suppress pelvic pain. Although PD-1 is classically recognized as an inhibitory immune checkpoint in T cells [3], accumulating work demonstrates that PD-1 is expressed in peripheral sensory neurons and regulates

nociceptive excitability [10; 36]. Here, we show that PD-1 is present across sensory and central nervous system tissues and is dynamically upregulated by SELTA in dorsal root ganglion (DRG) neurons.

SELTA enhanced PD-1 expression and phosphorylation in sensory neurons and colocalized with TLR2 at neuronal membranes. Importantly, SELTA increased phosphorylation of PD-1 at tyrosine 248 (Y248), a residue essential for the recruitment of SHP-2 and initiation of downstream inhibitory signaling [1]. The kinase(s) responsible for Y248 phosphorylation in response to SELTA remain unknown and are under investigation. Although bacterial lipoteichoic acids are known TLR2 ligands in epithelial and immune contexts [21], downstream activation of PD-1 signaling by such molecules has not been previously described. The mechanistic framework summarized in Figure 8 supports a model in which SELTA binds TLR2 and enhances PD-1 phosphorylation at Y248, ultimately reducing sensory neuron activation.

A key and novel finding of this study is the identification of SELTA as an exogenous, non–PD-L1/PD-L2 activator of PD-1 signaling. Canonical PD-1 activation is mediated by host-derived PD-L1 or PD-L2 [3; 7]. In contrast, SELTA is a commensal microbe–derived molecule that lacks structural homology to these ligands yet induces PD-1 phosphorylation and suppresses neuronal excitability. To our knowledge, this is the first demonstration that a commensal-derived molecule can activate PD-1 signaling in sensory neurons, expanding the known repertoire of PD-1 regulatory inputs.

The biological origin of SELTA is particularly notable in the context of *S. epidermidis* biology. *S. epidermidis* is a dominant human commensal that produces defined bioactive molecules capable of modulating host epithelial and immune function. Prior work has

shown that *S. epidermidis* products shape inflammatory responses, modulate TLR2 signaling, and contribute to barrier homeostasis [11; 20]. The demonstration that a purified *S. epidermidis* molecule can also modulate sensory neuron signaling broadens the scope of commensal–host interactions and highlights the possibility that commensal-derived factors influence neuroimmune regulation in peripheral tissues.

Using sensory neuron–specific PD-1 conditional knockout mice, we found that PD-1 expression in nociceptors is required for SELTA-mediated analgesia. SELTA failed to reduce pelvic tactile allodynia in Advillin-Cre–driven PD-1 knockouts, despite normal baseline behavior across anxiety-like, locomotor, exploratory, and cognitive assays. These results indicate that SELTA's analgesic effect depends on direct neuronal PD-1 signaling rather than indirect or systemic mechanisms.

At the cellular level, SELTA suppressed ATP-evoked intracellular Ca^{2+} elevations in DRG neurons, a robust indicator of sensory neuron activation [7]. This effect was abolished by PD-1 neutralizing antibody and restored when the antibody was preincubated with a PD-1 control peptide, demonstrating both PD-1 dependence and specificity. These observations align with mechanistic studies showing that PD-1–SHP-2 signaling suppresses excitatory ion channel activity and downstream neuronal activation pathways.

SELTA also increased PD-1 expression in prostate-innervating sensory fibers, including βIII-tubulin–positive and CGRP-positive axons, suggesting that PD-1–mediated modulation occurs at both somatic and peripheral terminals of nociceptors. Given that chronic prostatitis/chronic pelvic pain syndrome features persistent pelvic afferent sensitization and limited non-opioid treatment options, these findings identify neuronal PD-1 as a targetable checkpoint pathway for analgesic development.

Several questions remain. The identity of the kinase(s) mediating Y248 phosphorylation in neurons is unknown. Additional work is required to define the downstream signaling components—such as SHP-2 recruitment dynamics, ion channel targets, or purinergic signaling changes—that mediate SELTA's inhibitory actions. Although intraurethral SELTA was effective in mice, translational development will require evaluation of safety, formulation, and pharmacokinetics in humans.

Together, these findings identify SELTA as the first commensal-derived activator of neuronal PD-1 signaling and demonstrate that sensory neuron PD-1 is essential for SELTA-mediated analgesia. Through enhanced PD-1 expression, Y248 phosphorylation, and suppression of calcium mobilization, SELTA engages a neuronal checkpoint pathway that attenuates pelvic pain. The pathway summarized in Figure 8 highlights PD-1 activation as a potential non-opioid therapeutic strategy for chronic pelvic pain disorders.

Figure Legends

Figure 1. Basal neuronal PD-1 expression and SELTA-induced upregulation in sensory and immune tissues. (A) RT-PCR analysis of *Pdcd1* (PD-1) mRNA expression across splenocytes, lymph nodes, prostate, dorsal root ganglia (DRG), spinal cord, thalamus, hippocampus, and cortex. (B) qPCR quantification of *Pdcd1* mRNA in DRG from control versus SELTA-treated (100ng) mice. (C) Ex vivo DRG cultures showing PD-1 immunoreactivity in untreated (control) and SELTA-treated (100 ng/mL, 24 h) neurons. PD-1 (green) and NeuN (white) staining identify neuronal PD-1 expression. Scale bar = 30 μm. (D&E) Distribution of PD-1 immunoreactivity intensity across neuronal size

classes in control and SELTA-treated DRG. (F) Quantification of overall PD-1 immunoreactivity in DRG neurons from control and SELTA-treated mice. (G) Quantification of PD-1 immunoreactivity normalized to NeuN in DRG neurons from control and SELTA-treated mice. For all quantitative analyses, Student's *t*-test was used for two-group comparisons and two-way ANOVA for analyses involving multiple groups. $P < 0.05$; $P < 0.01$; $P < 0.001$; $P < 0.0001$. $n = 3–4$ per group. Abbreviations: NeuN, neuronal nuclear antigen; DRG, dorsal root ganglion; ANOVA, analysis of variance.

Figure 2. SELTA engages TLR2 on sensory neurons and enhances PD-1 phosphorylation.

(A) Representative confocal images showing exogenous SELTA binding to TLR2 on DRG neurons. Colocalization of SELTA with TLR2 and phosphorylated PD-1 (pPD-1) is indicated by purple arrows (somatic localization) and purple arrowheads (pre-synaptic or synapse-like regions). Scale bar = 20 μm. (B) Ex vivo DRG cultures showing pPD-1 (green) and NeuN (red) immunoreactivity in control (top) and SELTA-treated (100 ng/mL, 24 h; bottom) preparations. Scale bar = 30 μm. (C) Quantification of pPD-1 immunoreactivity across neuronal size classes in control and SELTA-treated DRG. (D) pPD-1 immunoreactivity normalized to NeuN in control and SELTA-treated DRG. For all quantitative analyses, Student's *t*-test was used for two-group comparisons, and two-way ANOVA was used for analyses involving more than two groups. $P < 0.05$; $P < 0.01$; $P < 0.001$; $P < 0.0001$. $n = 3–4$ per group. Abbreviations: pPD-1, phosphorylated programmed cell death-1; NeuN, neuronal nuclear antigen; DRG, dorsal root ganglion; ANOVA, analysis of variance.

Figure 3. SELTA attenuates pelvic allodynia in EAP mice with both single and repeated dosing and exhibits a concentration-dependent effect. (A) Schematic of the experimental design illustrating induction of experimental autoimmune prostatitis (EAP), timing of weekly behavioral assessments, and SELTA administration. SELTA was delivered intraurethrally on days 21 and 70. (B) Early-phase behavioral response extracted from panel C, showing pelvic tactile allodynia over the first 42 days and highlighting the effect of the first SELTA instillation at day 21. (C) Long-term pelvic tactile allodynia in saline-treated mice, EAP mice, and EAP mice receiving SELTA on days 21 and 70. Behavioral responses were assessed every 7 days up to day 119 and expressed as percentage change in response frequency relative to baseline. (D) Single-dose intraurethral SELTA dose–response study (0.01, 1, 10, or 100 μM) in EAP mice. Pelvic tactile allodynia was monitored over 7 days following treatment, and the results are displayed as percent difference relative to untreated EAP controls. For all behavioral analyses, two-way ANOVA with Tukey's multiple comparisons test was used. $P < 0.05$; P < 0.01; $P < 0.001$. Group sizes were 5–10 mice per condition. Abbreviations: EAP, experimental autoimmune prostatitis; SELTA, staphylococcal lipoteichoic acid analog; ANOVA, analysis of variance.

Figure 4. SELTA increases PD-1 expression in prostate nerve fibers of EAP mice. (A) RNA in situ hybridization combined with immunofluorescence demonstrates increased *Pdcd1* (PD-1) mRNA expression in the prostates of EAP mice treated with SELTA compared with EAP-only mice. Elevated PD-1 mRNA levels correspond with increased PD-1 immunoreactivity in adjacent sections. Scale bar=20 μm (B) Representative immunofluorescent images showing enhanced PD-1 (red)

immunoreactivity colocalized with βIII-tubulin–positive nerve fibers (green) in the prostatic stroma of EAP mice treated with SELTA compared with EAP-only controls (day 28, seven days after SELTA instillation). High-magnification images (right) correspond to the dashed regions in the left panels. White arrows indicate nerve fiber bundles exhibiting increased PD-1 signal. PD-1–positive nerve terminals are also evident around the epithelial layer. Short yellow arrows denote blood-derived cells with high PD-1 expression present in the lumen. Scale bar=20 and 10μm respectively on the left and right panels. (C) Representative immunofluorescent images showing PD-1 (red) colocalized with CGRP-positive sensory nerve fibers (green) in the prostatic stroma of EAP versus EAP+SELTA mice (day 28). Lower panels show high-magnification images of the dashed regions above. White arrows indicate CGRP-positive fibers with increased PD-1 labeling following SELTA treatment. Scale bar=50 and 20μm respectively on the upper and bottom panels.

Figure 5. Generation of the PD-1 conditional knockout (CKO) mouse and confirmation of PD-1 knockdown in sensory neurons. (A) The breeding schematic for generation of sensory-specific PD-1 CKO mice involved crossing floxed PD-1 and somatic sensory neuron-specific advillin promotor-controlled Cre mice. (B) Confirmation of PD-1 knockdown advillin-positive periphery sensory neurons was the CKO was done with PD-1 immunofluorescent staining. DRG from PD-1$^{f/f}$ mice was incubated with anti-PD-1 antibody with or without a PD-1 blocking peptide to establish specificity of PD-1 staining. Knockdown of PD-1 expression was then confirmed in Advil^{cre}-PD-1$^{f/f}$ mouse DRG. Specificity of the knockdown to sensory neurons was verified by showing reduced expression in NeuN expressing cells but not in IBA-1-positive cells (white arrowheads). Scale bar=25 μm.

Figure 6. Neuronal PD-1 is required for SELTA-induced attenuation of pelvic allodynia in EAP mice. (A) Pelvic tactile allodynia in EAP-treated PD-1$^{f/f}$ mice. EAP was allowed to develop for 50 days before mice received a single intraurethral SELTA instillation. Pelvic tactile hypersensitivity was then assessed at 1, 3, 5, and 7 days after SELTA treatment using a graded series of von Frey filaments. Data are expressed as percentage increase in response frequency relative to baseline for each filament force. (B) Pelvic tactile allodynia in EAP-treated PD-1$^{f/f}$;Advillin-Cre mice subjected to the same protocol. EAP was allowed to progress for 50 days, followed by intraurethral SELTA instillation and allodynia assessment at 1-, 3-, 5-, and 7-days post-treatment. (C) Comparison of SELTA efficacy between genotypes, displayed as the percent difference in SELTA-induced reduction of pelvic allodynia in PD-1$^{f/f}$ versus PD-1$^{f/f}$;Advillin-Cre mice across the 1–7-day (equal to the window from day-50 to day-57) post-treatment window. For statistical analysis, Student's *t*-test was used for comparisons between two groups, and two-way ANOVA was used for analyses involving more than two groups. $P < 0.05$; P < 0.01. n = 9-11 mice per group. Abbreviations: EAP, experimental autoimmune prostatitis; SELTA, staphylococcal lipoteichoic acid analog; ANOVA, analysis of variance.

Figure 7. SELTA inhibits ATP-evoked Ca^{2+} responses in DRG neurons, and this effect is reversed by PD-1 neutralization and restored by PD-1 peptide competition. (A–D) Primary DRG sensory neurons were stimulated with 20 μM ATP, and intracellular calcium levels were monitored using the F340/F380 fluorescence ratio. Baseline values were recorded for at least 60 seconds before ATP application. Peak ATP-evoked calcium responses were calculated as the difference between baseline and the average maximal F340/F380 ratio within the 10-second post-stimulation window. SELTA pretreatment

significantly reduced ATP-induced intracellular Ca^{2+} elevations compared with untreated controls (A). This inhibitory effect was abolished when neurons were pretreated with a PD-1 neutralizing antibody (anti-PD-1), demonstrating that SELTA's calcium-suppressive effect requires intact PD-1 signaling (B). When the PD-1 neutralizing antibody was pre-incubated with a PD-1 control peptide (CP + aPD-1 + SELTA), antibody neutralization was blocked, and SELTA's inhibitory effect on ATP-evoked Ca^{2+} responses was restored (C, D). These results show that SELTA functionally suppresses neuronal calcium mobilization—a key marker of sensory neuron activation—in a PD-1–dependent and PD-1–specific manner.

Figure 8. Proposed model: SELTA engages TLR2–PD-1 signaling to suppress sensory neuron activation. SELTA binds to TLR2 on sensory neurons and promotes PD-1 phosphorylation. PD-1 activates downstream signaling involving SHP-1/SHP-2 which are phosphatases that can act on key ion channels controlling sensory neuron firing [36]. SHP-1/SHP-2–dependent signaling suppresses neuronal excitability by dephosphorylating and inhibiting voltage-gated sodium channels (NaV) and by enhancing potassium currents, including through TREK family K2P channels [2], which stabilize the resting membrane potential. PD-1-SHP-1 signaling also directly modulates TRPV channels, with SHP-1–mediated dephosphorylation of TRPV1 known to blunt inflammatory hypersensitivity [35]. PD-1 can also mediate interaction with the mu (μ) opioid receptor (MOR) to modulate endogenous pain signaling in sensory neurons [34]. SELTA mediated activation of PD-1 activates SHP-1 and SHP-2 and reduces intracellular Ca^{2+} mobilization in response to excitatory stimuli such as ATP. This inhibitory effect is lost when PD-1 is neutralized and restored when neutralization is blocked by a PD-1

control peptide, supporting a PD-1–specific mechanism. Together, the model illustrates how SELTA activation of neuronal PD-1 dampens sensory neuron excitability and contributes to reduced pelvic pain behaviors.

Supplementary Figure S1. SELTA directly upregulates PD-1 in purified DRG neurons and selectively increases the PD-1Δex3 splice variant. (A) Schematic representation of mouse *Pdcd1* exon structure and splice variants analyzed by qPCR, including full-length PD-1 and the Δex2, Δex3, Δex2,3, Δex2,3,4, and Δ42 isoforms. Colored bars indicate exon composition and primer positions used for isoform-specific amplification. (B) Representative RT-PCR analysis of *Pdcd1* expression in purified primary DRG neuron cultures treated with vehicle, SELTA, TNFα, or SELTA plus TNFα. (C, D) qPCR analysis of the PD-1Δex3 splice variant (C) and total *Pdcd1* (D) in DRG neurons subjected to thapsigargin-induced ER stress with or without SELTA treatment. SELTA significantly increased total *Pdcd1* and PD-1Δex3 expression, whereas other splice variants remained unchanged or below the level of detection.

Supplementary Figure S2. Baseline behavioral characterization of PD-1 sensory neuron–specific conditional knockout mice. Baseline behavioral assays were performed in 5–7-week-old PD-1$^{f/f}$ (WT) and PD-1$^{f/f}$;Advillin-Cre (CKO) mice (n = 9 per genotype) to confirm that sensory-neuron PD-1 deletion does not alter general behavior. (A) Dark–light box test showing similar time spent in the light compartment in WT and CKO mice. (B) Y-maze spontaneous alternation showing comparable working memory and exploratory behavior across genotypes. (C) Novel object recognition test demonstrating similar discrimination indices in WT and CKO mice. (D) Open field test

showing comparable center-time percentages, indicating no differences in baseline locomotor or anxiety-related behavior.

REFERENCES

[1] Bardhan K, Aksoylar HI, Le Bourgeois T, Strauss L, Weaver JD, Delcuze B, Charest A, Patsoukis N, Boussiotis VA. Phosphorylation of PD-1-Y248 is a marker of PD-1-mediated inhibitory function in human T cells. Sci Rep 2019;9(1):17252.

[2] Chen G. PD-L1 inhibits acute and chronic pain by suppressing nociceptive neuron activity via PD-1. Nature Neuroscience 2017;20(7):917-926.

[3] Chen G, Kim YH, Li H, Luo H, Liu DL, Zhang ZJ, Lay M, Chang W, Zhang YQ, Ji RR. PD-L1 inhibits acute and chronic pain by suppressing nociceptive neuron activity via PD-1. Nat Neurosci 2017;20(7):917-926.

[4] Clemens JQ, Markossian T, Calhoun EA. Comparison of economic impact of chronic prostatitis/chronic pelvic pain syndrome and interstitial cystitis/painful bladder syndrome. Urology 2009;73(4):743-746.

[5] Cyril AC, Jan RK, Radhakrishnan R. Pain in chronic prostatitis and the role of ion channels: a brief overview. Br J Pain 2022;16(1):50-59.

[6] Czeschik JC, Hagenacker T, Schäfers M, Büsselberg D. TNF-α differentially modulates ion channels of nociceptive neurons. Neuroscience letters 2008;434(3):293-298.

[7] Deng D, Zhang T, Ma L, Zhao W, Huang S, Wang K, Shu S, Chen X. PD-L1/PD-1 pathway: a potential neuroimmune target for pain relief. Cell & Bioscience 2024;14(1):51.

[8] Ennaceur A, Delacour J. A New One-Trial Test for Neurobiological Studies of Memory in Rats .1. Behavioral-Data. Behav Brain Res 1988;31(1):47-59.

[9] Huang Y, Zang Y, Zhou L, Gui W, Liu X, Zhong Y. The role of TNF-alpha/NF-kappa B pathway on the up-regulation of voltage-gated sodium channel Nav1. 7 in DRG neurons of rats with diabetic neuropathy. Neurochemistry international 2014;75:112-119.

[10] Jiang Y. PD-1 regulates the anti-tumor immune function of macrophages through JAK2–STAT3 signaling. Journal of Translational Medicine 2025.

[11] Lai Y, Di Nardo A, Nakatsuji T, Leichtle A, Yang Y, Cogen AL, Wu Z-R, Hooper LV, Schmidt RR, von Aulock S, Radek KA, Huang C-M, Ryan AF, Gallo RL. Commensal bacteria regulate Toll-like receptor 3–dependent inflammation after skin injury. Nature Medicine 2009;15(12):1377-1382.

[12] Laird JMA, Martinez-Caro L, Garcia-Nicas E, Cervero F. A new model of visceral pain and referred hyperalgesia in the mouse. Pain 2001;92(3):335-342.

[13] Meerschaert KA, Edwards BS, Epouhe AY, Jefferson B, Friedman R, Babyok OL, Moy JK, Kehinde F, Liu C, Workman CJ, Vignali DAA, Albers KM, Koerber HR, Gold MS, Davis BM, Scheff NN, Saloman JL. Neuronally expressed PDL1, not PD1, suppresses acute nociception. Brain, Behavior, and Immunity 2022;106:233-246.

[14] Miedel CJ, Patton JM, Miedel AN, Miedel ES, Levenson JM. Assessment of Spontaneous Alternation, Novel Object Recognition and Limb Clasping in Transgenic Mouse Models of Amyloid-beta and Tau Neuropathology. J Vis Exp 2017(123).

[15] Mo YJ, Kim YS, Kim MS, Lee YI. Advantages of Adult Mouse Dorsal Root Ganglia Explant Culture in Investigating Myelination in an Inherited Neuropathic Mice Model. Methods Protoc 2022;5(4).

[16] Murphy SF, Anker JF, Mazur DJ, Hall C, Schaeffer AJ, Thumbikat P. Role of gram-positive bacteria in chronic pelvic pain syndrome (CPPS). Prostate 2019;79(2):160-167.
[17] Murphy SF, Hall C, Done JD, Schaeffer AJ, Thumbikat P. A prostate derived commensal Staphylococcus epidermidis strain prevents and ameliorates induction of chronic prostatitis by UPEC infection. Sci Rep 2018;8(1):17420.
[18] Murphy SF, Schaeffer AJ, Done JD, Quick ML, Acar U, Thumbikat P. Commensal bacterial modulation of the host immune response to ameliorate pain in a murine model of chronic prostatitis. Pain 2017;158(8):1517-1527.
[19] Murphy SF, Schaeffer AJ, Thumbikat P. Immune mediators of chronic pelvic pain syndrome. Nat Rev Urol 2014;11(5):259-269.
[20] Naik S, Bouladoux N, Linehan JL, Han SJ, Harrison OJ, Wilhelm C, Conlan S, Himmelfarb S, Byrd AL, Deming C, Quinones M, Brenchley JM, Kong HH, Tussiwand R, Murphy KM, Merad M, Segre JA, Belkaid Y. Commensal-dendritic-cell interaction specifies a unique protective skin immune signature. Nature 2015;520(7545):104-108.
[21] Nilsen NJ, Vladimer GI, Stenvik J, Orning MP, Zeid-Kilani MV, Bugge M, Bergstroem B, Conlon J, Husebye H, Hise AG, Fitzgerald KA, Espevik T, Lien E. A role for the adaptor proteins TRAM and TRIF in toll-like receptor 2 signaling. J Biol Chem 2015;290(6):3209-3222.
[22] Paul M, Murphy SF, Hall C, Schaeffer AJ, Thumbikat P. Protease-activated receptor 2 activates CRAC-mediated Ca2+ influx to cause prostate smooth muscle contraction. FASEB Bioadv 2019;1(4):255-264.
[23] Quick ML, Done JD, Thumbikat P. Measurement of tactile allodynia in a murine model of bacterial prostatitis. J Vis Exp 2013(71):e50158.
[24] Rudick CN, Schaeffer AJ, Thumbikat P. Experimental autoimmune prostatitis induces chronic pelvic pain. Am J Physiol Regul Integr Comp Physiol 2008;294(4):R1268-1275.
[25] Semina E, Rubina K, Sysoeva V, Rysenkova K, Klimovich P, Plekhanova O, Tkachuk V. Urokinase and urokinase receptor participate in regulation of neuronal migration, axon growth and branching. Eur J Cell Biol 2016;95(9):295-310.
[26] Simon P, Dupuis R, Costentin J. Thigmotaxis as an Index of Anxiety in Mice - Influence of Dopaminergic Transmissions. Behav Brain Res 1994;61(1):59-64.
[27] Sleigh JN, West SJ, Schiavo G. A video protocol for rapid dissection of mouse dorsal root ganglia from defined spinal levels. BMC Research Notes 2020;13(1):302.
[28] Stettner M, Wolffram K, Mausberg AK, Wolf C, Heikaus S, Derksen A, Dehmel T, Kieseier BC. A reliable in vitro model for studying peripheral nerve myelination in mouse. J Neurosci Methods 2013;214(1):69-79.
[29] Sutcliffe S, Newcomb C, Bradley CS, Clemens JQ, Erickson B, Gupta P, Lai HH, Naliboff B, Strachan E, Stephens-Shields A. Associations Between Urological Chronic Pelvic Pain Syndrome Symptom Flares, Illness Impact, and Health Care Seeking Activity: Findings From the Multidisciplinary Approach to the Study of Chronic Pelvic Pain Symptom Patterns Study. J Urol 2023:101097JU0000000000003155.
[30] Tamura R, Nemoto T, Maruta T, Onizuka S, Yanagita T, Wada A, Murakami M, Tsuneyoshi I. Up-regulation of NaV1. 7 sodium channels expression by tumor necrosis factor-α in cultured bovine adrenal chromaffin cells and rat dorsal root ganglion neurons. Anesthesia & Analgesia 2014;118(2):318-324.

[31] Tyagi S, Higerd-Rusli GP, Ghovanloo M-R, Dib-Hajj F, Zhao P, Liu S, Kim D-H, Shim JS, Park K-S, Waxman SG, Choi J-S, Dib-Hajj SD. Compartment-specific regulation of NaV1.7 in sensory neurons after acute exposure to TNF-α. Cell Reports 2024;43(2):113685.
[32] Valdez-Morales EE, Sánchez-Navarro CA, Reyes-Pavón D, Barrios-Garcia T, Ochoa-Cortes F, Barajas-Espinosa A, Barragán-Iglesias P, Guerrero-Alba R. TNF-α enhances sensory DRG neuron excitability through modulation of P2X3 receptors in an acute colitis model. Frontiers in Immunology 2022;13:872760.
[33] Wang T, Bergmans R, Minc A, Krieger J, Harris RE, Lai HH, Clemens JQ, Harte SE, Kaplan C, Williams DA, Naliboff B, Gallop R, Till S, Schrepf A. High-impact Chronic Pain in a Cohort of Urologic Chronic Pelvic Pain Syndrome Patients: A Retrospective MAPP Research Network Study. Clin J Pain 2025;41(4).
[34] Wang Z, Jiang C, He Q, Matsuda M, Han Q, Wang K, Bang S, Ding H, Ko MC, Ji RR. Anti-PD-1 treatment impairs opioid antinociception in rodents and nonhuman primates. Sci Transl Med 2020;12(531).
[35] Xiao X, Zhao XT, Xu LC, Yue LP, Liu FY, Cai J, Liao FF, Kong JG, Xing GG, Yi M, Wan Y. Shp-1 dephosphorylates TRPV1 in dorsal root ganglion neurons and alleviates CFA-induced inflammatory pain in rats. Pain 2015;156(4):597-608.
[36] Zhao J, Roberts A, Wang Z, Savage J, Ji RR. Emerging Role of PD-1 in the Central Nervous System and Brain Diseases. Neurosci Bull 2021.

Table 1: Primer Sequences and PCR Conditions for Nested PCR Amplification of the Full-Length PD-1 Gene

Primer Set		Sequence (5' ⟶3')	Amplicon Size (bp)	Annealing Temperature (°C)
Outer	Forward	TGAGCTGGCAATCAGGGTG	760	60
	Reverse	CCATCAGCTGAGCCCCTAC		
Inner	Forward	GGCAATCAGGGTGGCTT	616	60
	Reverse	TAGGCCACACTAGGGACAGG		

Table 2: Primer Sequences for qPCR Detection of Mouse PD-1 Gene Splice Variants

PD-1 primers for QPCR	Forward	Forward primer sequence composition and position				Reverse	
FL-ms-PD1	5'-CTCGTGGTAACAGAGAGAAT-3'	ex2-3	487-506			5' TAGGGACAGGTGCTGCTGAA-3'	708-727
ms-PD-1Dex2	5'-GGCTTCTAGAGAGAATCCTG-3'	ex1	131-139	ex3	500-510	5'-GATACCAATGACCATGCCTTG-3	562-582
ms-PD-1Dex3	5'-GTGGTAACAGAGGCCAGAGG-3'	ex2	490-499	ex4	662-671	5'-TCATAGGCCACACTAGGGACA-3	720-740
ms-PD-1Dex2,3	5'-TGGCTTCTAGAGGCCAGAGGA-3'	ex1	130-139	ex4	662-672	5'-TCTTCTCTCGTCCCTGGAAG-3'	750-769
ms-PD-1Dex2,3,4	5'-TGGCTTCTAGAAGGAGGAGC-3'	ex1	130-139	ex5	697-706	5'-TCTTCTCTCGTCCCTGGAAG-3'	750-769
ms-PD-1D42	5'-GGCTTCTAGCCTGGCTCACA-3'	ex1	131-139	ex2	182-192	5'-CCTGTTGGGCAGCTGTATGA-3'	353-372

A

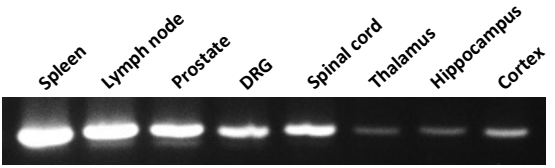
Spleen
Lymph node
Prostate
DRG
Spinal cord
Thalamus
Hippocampus
Cortex

B

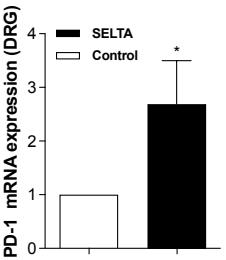
SELTA
Control
PD-1 mRNA expression (DRG)
0
1
2
3
4
*

C

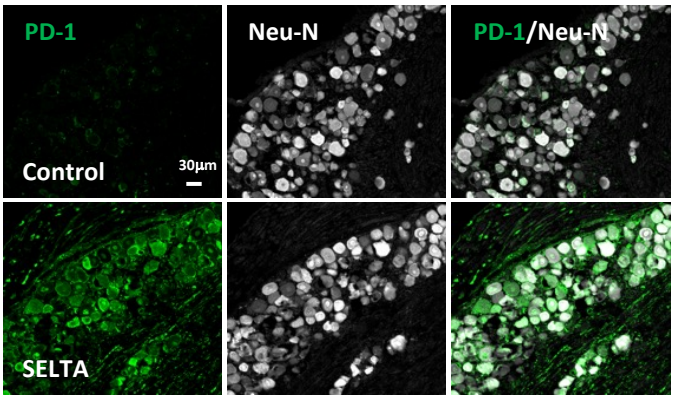
PD-1
Neu-N
PD-1/Neu-N
Control
30μm
SELTA

D

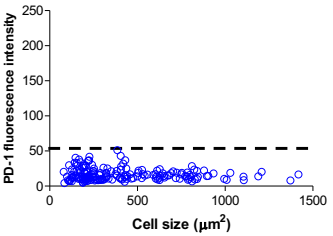
Control
PD-1 fluorescence intensity
0
50
100
150
200
250
0
500
1000
1500
Cell size (μm²)

E

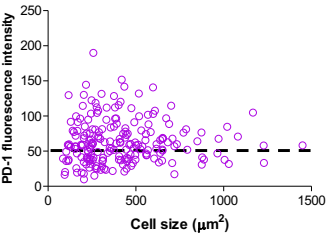
SELTA
PD-1 fluorescence intensity
0
50
100
150
200
250
0
500
1000
1500
Cell size (μm²)

F

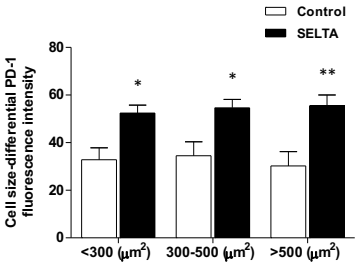
Control
SELTA
Cell size-differential PD-1 fluorescence intensity
0
20
40
60
80
*
*
**
<300 (μm²)
300-500 (μm²)
>500 (μm²)

G

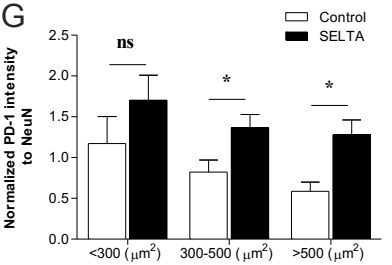
Control
SELTA
Normalized PD-1 intensity to NeuN
0.0
0.5
1.0
1.5
2.0
2.5
ns
*
*
<300 (μm²)
300-500 (μm²)
>500 (μm²)

A

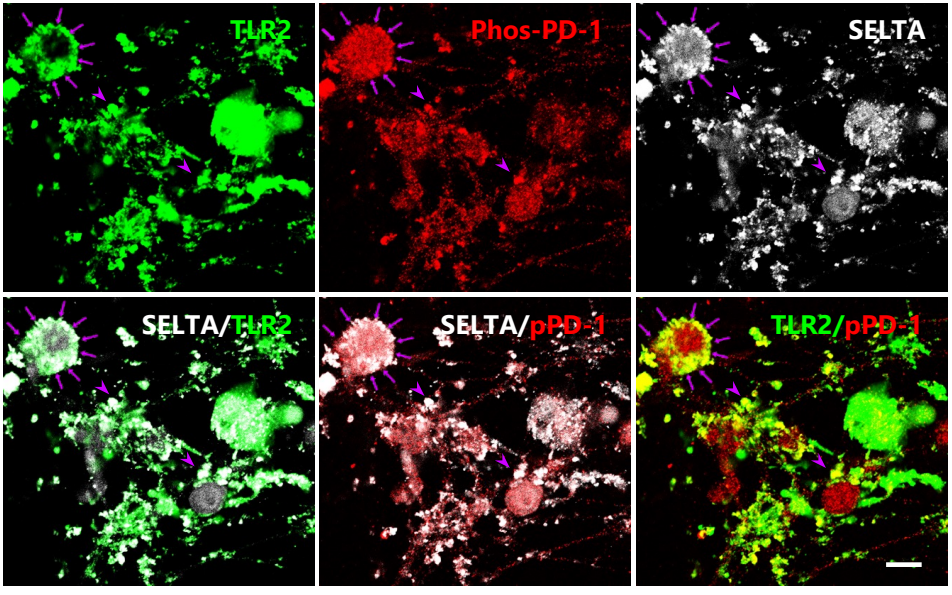
TLR2
Phos-PD-1
SELTA
SELTA/TLR2
SELTA/pPD-1
TLR2/pPD-1

B

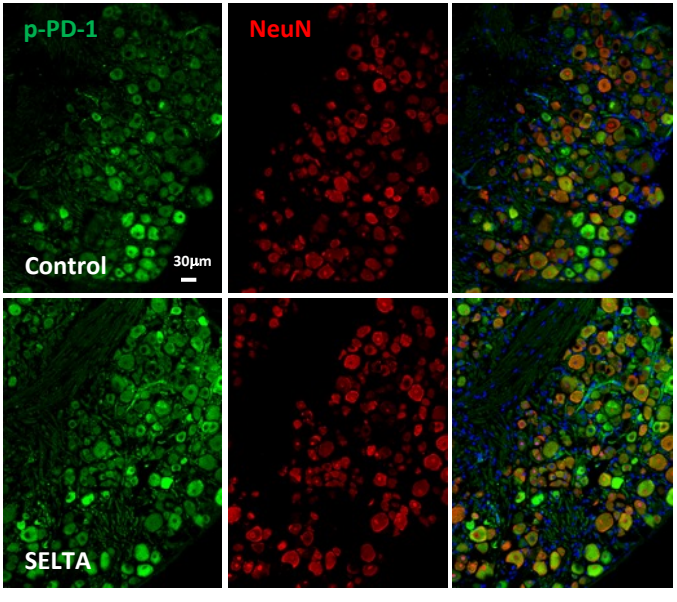
p-PD-1
NeuN
Control
30μm
SELTA

C

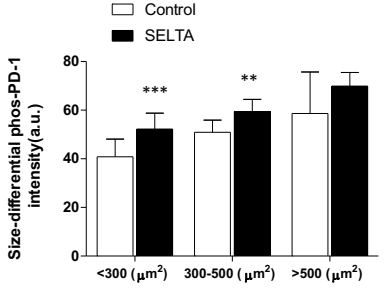
Control
SELTA
Size-differential phos-PD-1 intensity(a.u.)
80
60
40
20
0
***
**
<300 (μm²)
300-500 (μm²)
>500 (μm²)

D

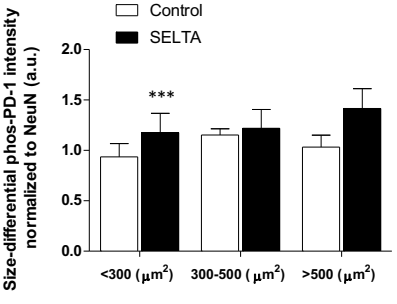
Control
SELTA
Size-differential phos-PD-1 intensity normalized to NeuN (a.u.)
2.0
1.5
1.0
0.5
0.0
***
<300 (μm²)
300-500 (μm²)
>500 (μm²)

A

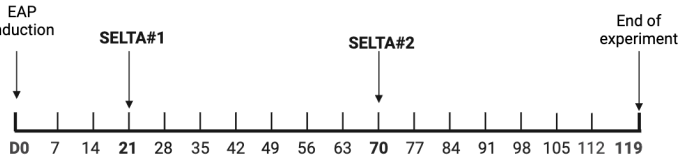
EAP induction
SELTA#1
SELTA#2
End of experiment
D0 7 14 21 28 35 42 49 56 63 70 77 84 91 98 105 112 119

B

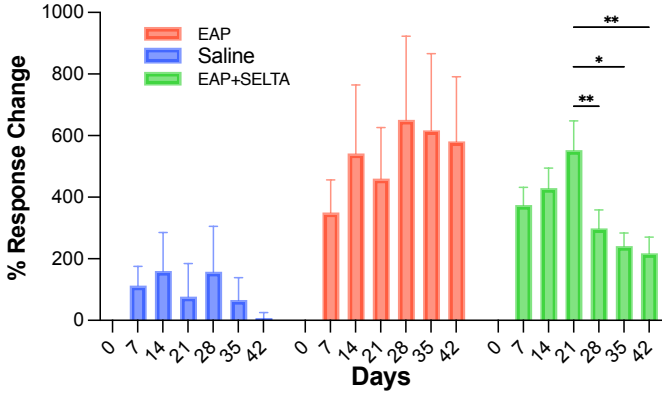
% Response Change
EAP
Saline
EAP+SELTA
Days

C

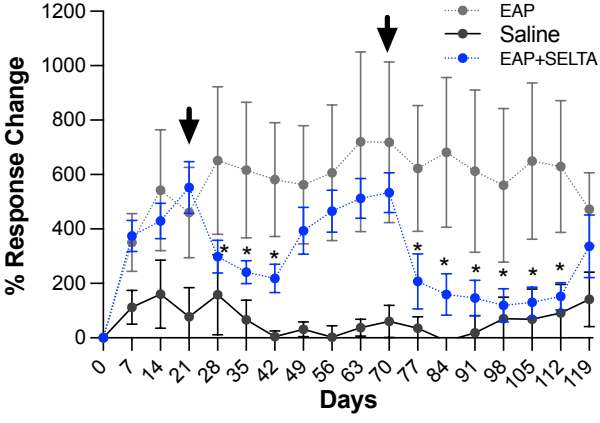
% Response Change
EAP
Saline
EAP+SELTA
Days

D

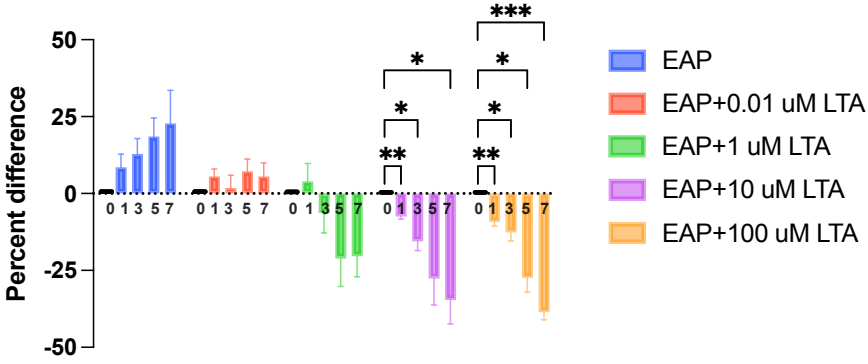
Percent difference
EAP
EAP+0.01 uM LTA
EAP+1 uM LTA
EAP+10 uM LTA
EAP+100 uM LTA

A

PD-1 mRNA in the prostate

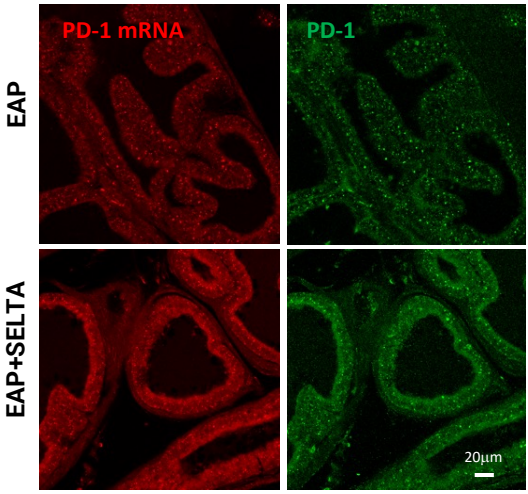

B

PD-1 expression in the prostate

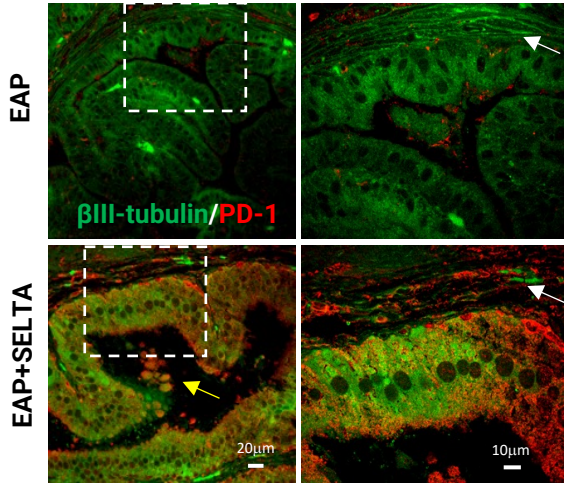

C

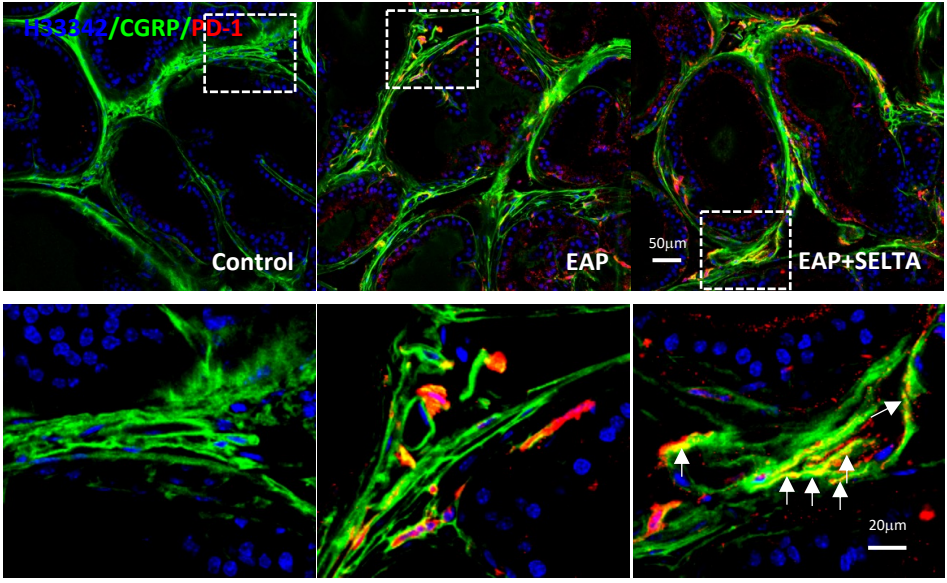

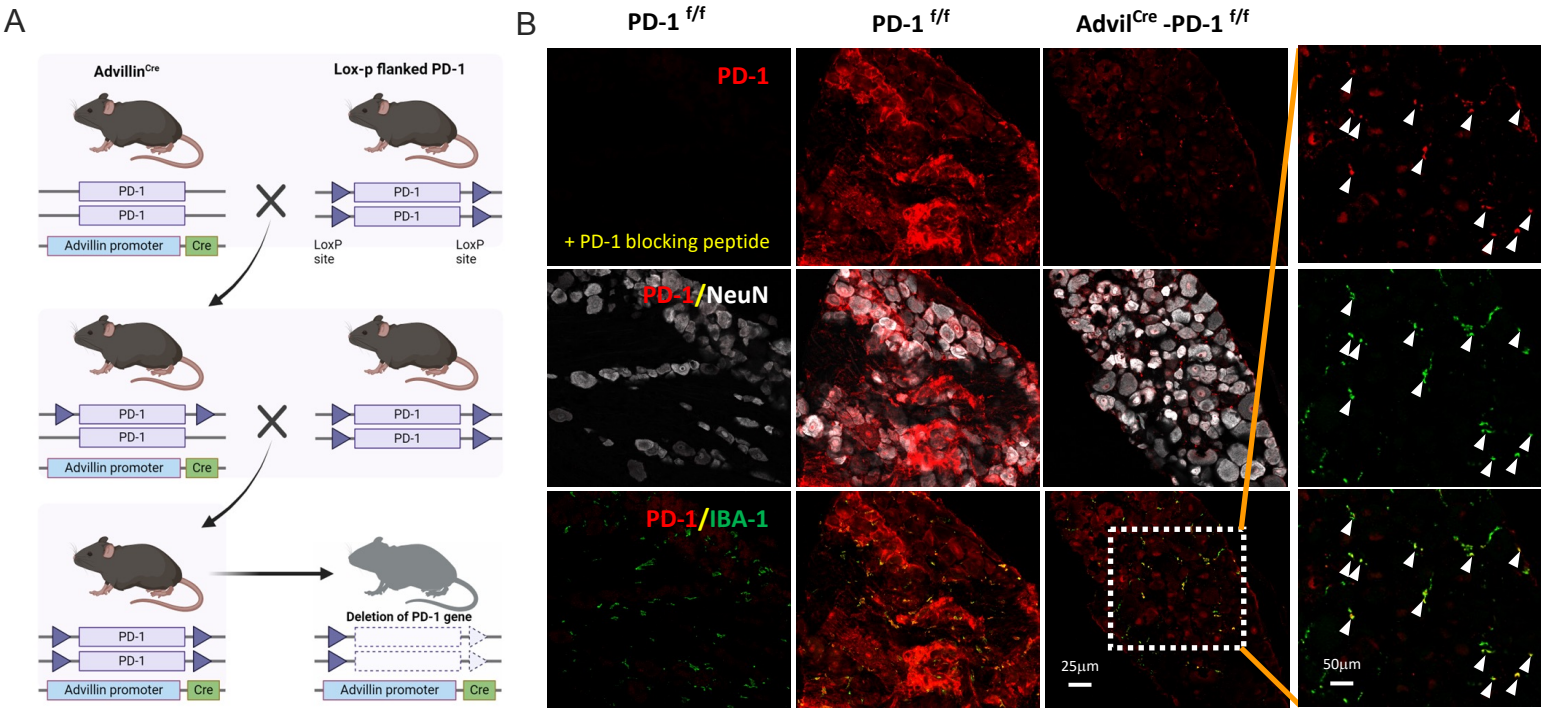
A
Advillin^Cre
Lox-p flanked PD-1
PD-1
PD-1
Advillin promoter
Cre
LoxP site
LoxP site
Deletion of PD-1 gene
B
PD-1 f/f
PD-1 f/f
AdvilCre -PD-1 f/f
PD-1
+ PD-1 blocking peptide
PD-1/NeuN
PD-1/IBA-1
25μm
50μm

A

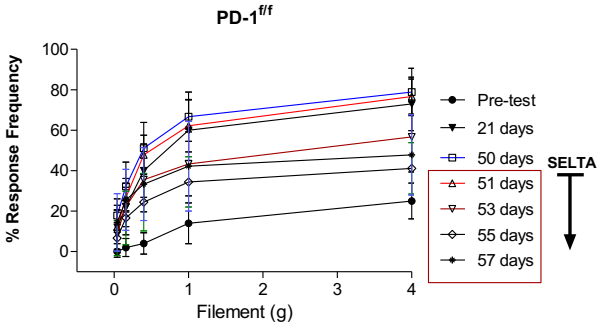
PD-1f/f
% Response Frequency
100
80
60
40
20
0
0
1
2
3
4
Filement (g)
Pre-test
21 days
50 days
51 days
53 days
55 days
57 days
SELTA

B

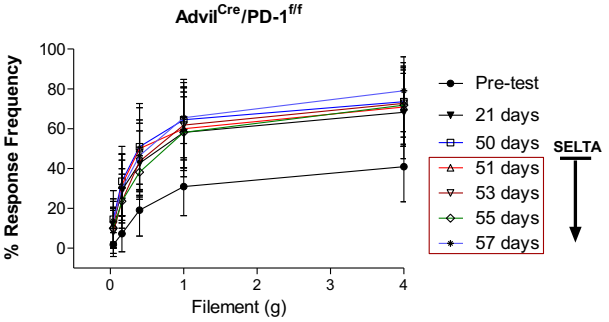
AdvilCre/PD-1f/f
% Response Frequency
100
80
60
40
20
0
0
1
2
3
4
Filement (g)
Pre-test
21 days
50 days
51 days
53 days
55 days
57 days
SELTA

C

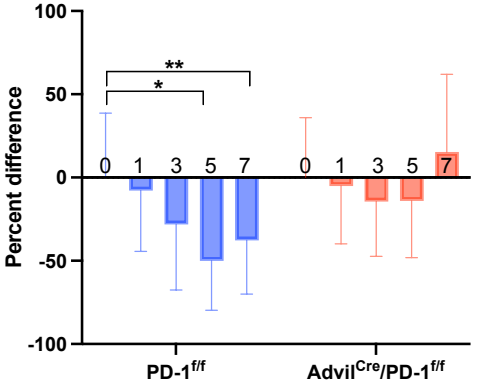
Percent difference
100
50
0
-50
-100
**
*
0
1
3
5
7
0
1
3
5
7
PD-1f/f
AdvilCre/PD-1f/f

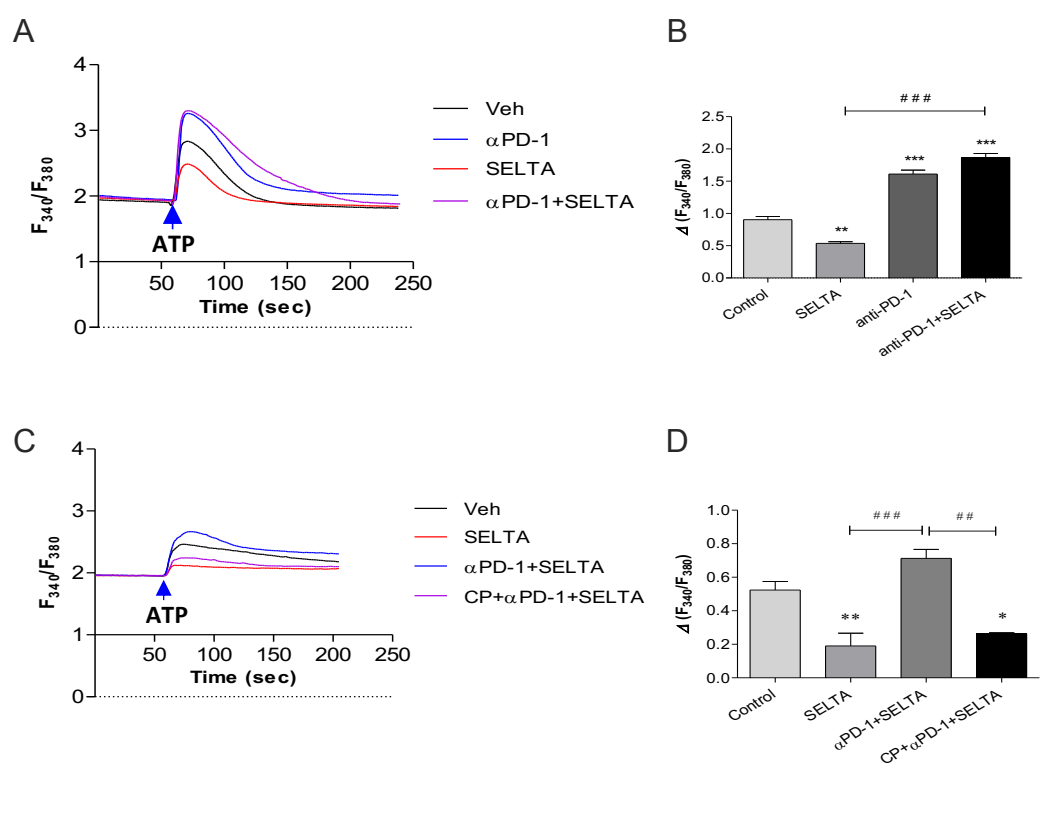
A
4
3
2
1
0
F340/F380
ATP
50
100
150
200
250
Time (sec)
Veh
αPD-1
SELTA
αPD-1+SELTA
B
###
2.5
2.0
1.5
1.0
0.5
0.0
Δ (F340/F380)
**
***
***
Control
SELTA
anti-PD-1
anti-PD-1+SELTA
C
4
3
2
1
0
F340/F380
ATP
50
100
150
200
250
Time (sec)
Veh
SELTA
αPD-1+SELTA
CP+αPD-1+SELTA
D
###
##
1.0
0.8
0.6
0.4
0.2
0.0
Δ (F340/F380)
**
*
Control
SELTA
αPD-1+SELTA
CP+αPD-1+SELTA

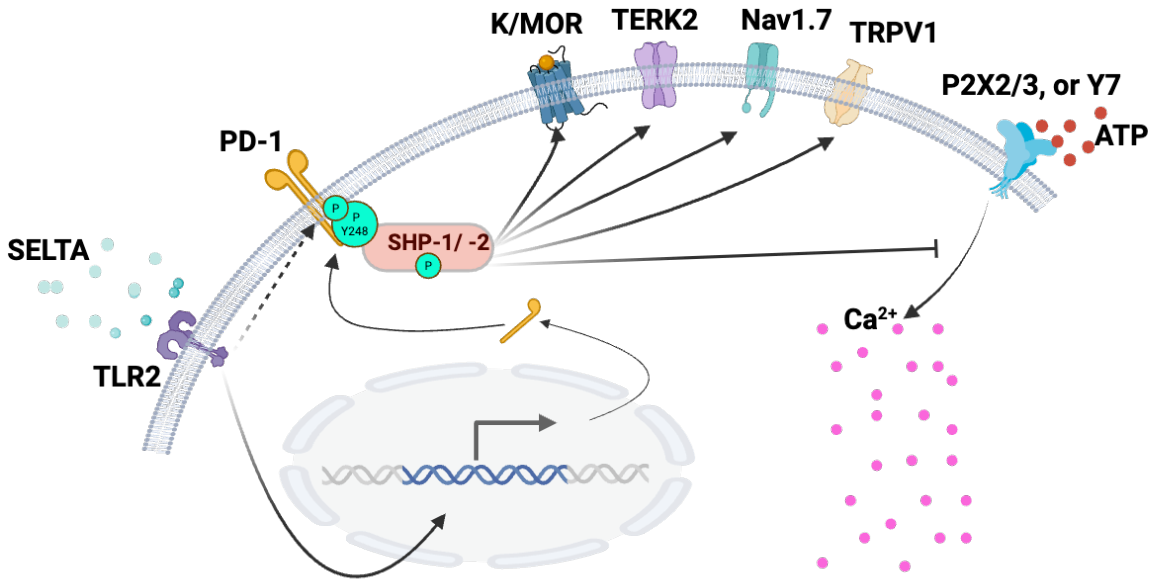
K/MOR
TERK2
Nav1.7
TRPV1
P2X2/3, or Y7
ATP
PD-1
P
P
Y248
SHP-1/ -2
P
SELTA
TLR2
Ca2+